Impact, Trapping, and Accommodation of Hydroxyl Radical and Ozone at Aqueous Salt Aerosol Surfaces. A Molecular Dynamics Study

Martina Roeselová,*,† Pavel Jungwirth,† Douglas J. Tobias,‡ and R. Benny Gerber‡,§

J. Heyrovský Institute of Physical Chemistry, Academy of Sciences of Czech Republic, and Center for Complex Molecular Systems and Biomolecules, Dolejškova 3, 18223 Prague, Czech Republic, Department of Chemistry, University of California, Irvine, California 92697-2025, and Department of Physical Chemistry and Fritz Haber Center for Molecular Dynamics, Hebrew University of Jerusalem, Jerusalem 91904, Israel

Received: May 8, 2003; In Final Form: August 14, 2003

Collisions of the gaseous hydroxyl (OH) radical and ozone (O_3) with the surfaces of sodium chloride or iodide solutions, as well as with the surface of neat water, were investigated by molecular dynamics simulations. The principal intent was to answer atmospherically relevant questions concerning the trapping and accommodation of the OH and O_3 species at the surface and their uptake into the bulk solution. Although trapping is substantial for both species, OH adsorbs and absorbs significantly better than O_3. Most of the trapped O_3 molecules desorb from the surface within 50 ps, whereas a significant fraction of OH radicals remains at the interface for time intervals exceeding 100 ps. The aqueous surface has also an orientational effect on the OH species, favoring geometries with the H atom pointing toward the aqueous bulk. The effect of the dissolved salt on the trapping efficiency is minor; therefore, most likely, atomic ions solvated in aqueous aerosols do not act as strong scavengers of reactive gases in the atmosphere. However, frequent and relatively long contacts between the adsorbed molecules and halide anions do occur, allowing for heterogeneous atmospheric chemistry in the interfacial layer.

1. Introduction

Aerosols of different types have long been recognized to have major roles in a variety of processes of atmospheric importance.[1,2] Processes on solid aerosols are generally considered to occur at the surface of the particle, whereas, for liquid aerosols, both homogeneous reactions and heterogeneous processes at the aerosol/air interface can be important, depending on the system.[3−10] Indeed, several atmospheric reactions of major interest have been attributed to heterogeneous chemistry that occurs at the aerosol surfaces.[3−6] Although, qualitatively, the evidence for the role of aerosols in atmospheric processes is strong, the microscopic mechanisms for the action of aerosols are poorly understood. To understand further the detailed mechanisms whereby processes at aerosol surfaces occur, it is desirable to understand the uptake of the relevant molecules by the aerosol droplet, to describe the accommodation of the molecule at the surface once trapped, and to explore the dynamics of the reactions that eventually occur. Such a level of understanding was attained for a range of processes at the gas/surface interface, especially for single-crystal surfaces. Rigorous, quantitative experiments using surface ultrahigh-vacuum (UHV) techniques, combined with theoretical simulations at the atomic level of detail, have often provided such insights.[11−13] The understanding of chemical dynamics at liquid/air surfaces is, generally, less advanced than that for single-crystal surfaces, but also major progress was made for such systems, often by the combination of microscopically sensitive experimental techniques with theoretical simulations, from an atomistic point of view.[14−18]

Our objective in this paper is to explore the dynamics of molecular interactions with liquid aerosol surfaces, using molecular dynamics (MD) simulations to describe the processes involved. Specifically, we shall explore the interaction of the atmospherically important species O_3 and OH with NaCl/water and related aqueous aerosols. There is strong evidence of an efficient release of chlorine in heterogeneous reactions at the surface of the aerosols.[3] In a previous paper, we explored the structure of the aerosols and suggested that an enhanced presence of negative ions at the surface may have a role in the mechanism.[19] In the present article, we investigate the uptake of molecules by the aerosol and study the accommodation dynamics and the behavior of the trapped species at the surface. These processes are of intrinsic interest, and it is hoped that understanding them will ultimately also explain/define the chemical reactions and their mechanisms.

First, we addressed the question concerning the probability that a gas-phase OH radical or an O_3 molecule with a thermal velocity adsorbs at the interface. Second, we examined the probabilities that molecules initially adsorbed at the surface remain for a certain duration in the interface layer, become solvated in the bulk, or desorb back into the gas phase. Specifically, we wanted to know how much time, on average, the adsorbed molecule spends on the surface before being desorbed again or becoming fully solvated. Third, we tested the suggestion that halide ions exposed on the surface might act as scavengers that attract reactive species from the gas phase.[19] Finally, we investigated to what extent the adsorbed OH radical comes into direct contact with halide ions present in the interface layer. In particular, we wanted to assess if the

* Author to whom correspondence should be addressed. E-mail: mroeselo@uci.edu. Currently with University of California, Irvine, CA.

† J. Heyrovský Institute of Physical Chemistry, Academy of Sciences of Czech Republic, and Center for Complex Molecular Systems and Biomolecules.

‡ University of California.

§ Hebrew University of Jerusalem.

10.1021/jp030592i CCC: $25.00
Published on Web 10/28/2003

occurrence and duration of the contacts between OH and Cl^- are sufficient to support the surface mechanism of molecular chlorine (Cl_2) production based on the formation of a $OH\cdots Cl^-$ complex.[19]

The structure of the paper is as follows. Details concerning modeling of the system and the simulation approach are described in Section 2. Results are presented and discussed in Section 3, and conclusions are summarized in Section 4.

2. Systems and Computational Methods

MD simulations were conducted for a OH radical or an O_3 molecule interacting with a water slab, either neat or containing sodium chloride (NaCl) at saturation (6.1 M) or sodium iodide (NaI) at a concentration of 1.2 M. In the laboratory experiment, the intent of which was to elucidate the reaction mechanism that leads to the production of Cl_2,[19] the NaCl concentration in the aqueous salt aerosol particles was equal to ~4.5 M, whereas, under atmospheric conditions, this concentration spans a broad interval, ranging from seawater concentrations to saturation. The concentration of NaI (1.2 M) was chosen to be approximately the same as that used in the experimental investigation of the uptake of ozone by aqueous solutions.[48]

To construct the slabs, a rectangular cell with dimensions of 30 Å × 30 Å × 100 Å was used; these cells contained 864 water molecules, 96 Na ions, and 96 Cl ions in the case of the saturated NaCl solution and 864 water molecules, 18 Na ions, and 18 I ions in the case of 1.2 M NaI solution. Application of such periodic boundary conditions at constant volume yielded an infinite slab with two open surfaces, perpendicular to the *z*-axis. For comparison, we also performed simulations with a slab of neat water. In this case, 864 water molecules in an identical simulation cell were used.

The MD simulations were performed using the AMBER 6 program package[20] with polarizable potentials.[21−24] Inclusion of atomic polarizabilities was shown to be crucial for the correct description of mixed halide anion−water clusters,[23,25] as well as aqueous salt solution/air interfaces.[19,26,27] The only difference between the force field reported in refs 19, 26, and 27 and that used in this work concerns the value of polarizability of the Cl ion. In the present simulations, we use a slightly higher value of 4.0 Å, which was suggested recently.[28]

In regard to the OH radical and O_3 molecule, the geometrical parameters were taken from the ab initio MP2/aug-cc-pvtz optimizations. The partial atomic charges were obtained at the MP2/6-31G level. All ab initio calculations were performed using the GAUSSIAN98 program package.[29−32] For the atomic polarizabilities of the O and H atoms of the hydroxyl radical, values equal to those used for the water molecule were used. The polarizability of the ozone molecule was obtained as a mean value of the diagonal elements of the polarizability tensor calculated at the MP2/aug-cc-pvtz level. One-third of this value was then assigned to each of the three O atoms of the ozone molecule. A test simulation, in which the entire polarizability of ozone was assigned to the central oxygen, was conducted, and no substantial difference between the two models was observed.

The force field parameters are summarized in Table 1. Checks against ab initio calculations show that this parametrization is satisfactory, but it slightly underestimates the $OH-H_2O$ binding, and somewhat overestimates the $Cl^- - H_2O$ binding. At the same time, the $OH-Cl^-$ binding is underestimated. It is, apparently, difficult to describe accurately the OH radical−water, and, particularly, the OH radical−halide anion interactions, by an empirical force field.

TABLE 1: Force Field Parameters

	q (e)	α (Å^3)	R_m (Å)	ϵ (kcal/mol)
Na^+	1.0	0.24	1.532	0.100
Cl^-	−1.0	4.00	2.509	0.118
I^-	−1.0	6.90	2.890	0.100
H_2O				
O	−0.73	0.528	1.798	0.156
H	0.365	0.170	0	0
OH				
O	−0.4	0.528	1.798	0.156
H	0.4	0.170	1.32	0.022
O_3				
O_{center}	0.12	0.770	1.798	0.156
O_{side}	−0.06	0.770	1.798	0.156

The trapping of the OH radical and O_3 at the air/solution interface was investigated by running a series of scattering trajectories. First, an equilibrated configuration of the salt solution or neat water slab has been produced by a 0.5-ns MD trajectory. Using this slab configuration, 25 initial configurations for the scattering trajectories were generated by placing the OH radical or O_3 molecule at random points in the *xy*-plane, 12.5 Å above the surface of the slab. To test whether the initial orientation of the hydroxyl radical, with respect to the surface, might have a role in the simulations, two orientations of OH were considered, both with the O−H bond along the *z*-axis (i.e., perpendicular to the surface): one with the O atom facing the surface, the other with the O atom pointing away from the surface. Because of the orientational effect of the interface on the OH radical (see Section 3), both sets of simulations provided statistically equivalent results for all slabs. In the case of ozone, only one initial orientation was considered, with the central O atom pointing away from the surface and the two side O atoms positioned symmetrically, with respect to the *z*-axis and facing the surface. The initial velocity of both the OH radical and the O_3 molecule was set to the most probable value from the corresponding Maxwell−Boltzmann distribution at 300 K, and scattering under five different impact angles (0°, 22.5°, 45°, 67.5°, and 85°) was investigated. Using these initial conditions, a total of 125 scattering trajectories, each of a duration of 100 ps, were generated for the OH and O_3 interaction with the saturated NaCl/water slab, with the neat water slab, and with the 1.2 M NaI/water slab.

System geometries were monitored every picosecond. Trajectories for which the OH radical or O_3 molecule spent 2 ps or less in the interfacial layer were classified as a scattering event, whereas the rest of the trajectories were considered as adsorption. The classification of whether, in a particular time step, the molecule is in the gas phase, in the interface layer, or in the bulk solution was based on the Solvent Accessible Surface Area (SASA) technique. The accessible surface of the incoming OH or O_3 particle was evaluated using the Lee and Richards algorithm[33] with a probe radius of 1.2 Å. Depending on the SASA value, the configurations were sorted into three sets: (1) solute fully exposed (i.e., in the gas phase), (2) solute partially solvated (i.e., in interface), and (3) solute fully solvated (i.e., in the aqueous bulk).

A constant temperature of 300 K was maintained throughout the simulations. A time step of 1 fs was used. All bond vibrations that involve H atoms were constrained using the SHAKE algorithm.[34] Intermolecular interactions were truncated at 12 Å. A smooth particle mesh Ewald method was used to account for the long-range electrostatic energies and forces.[35]

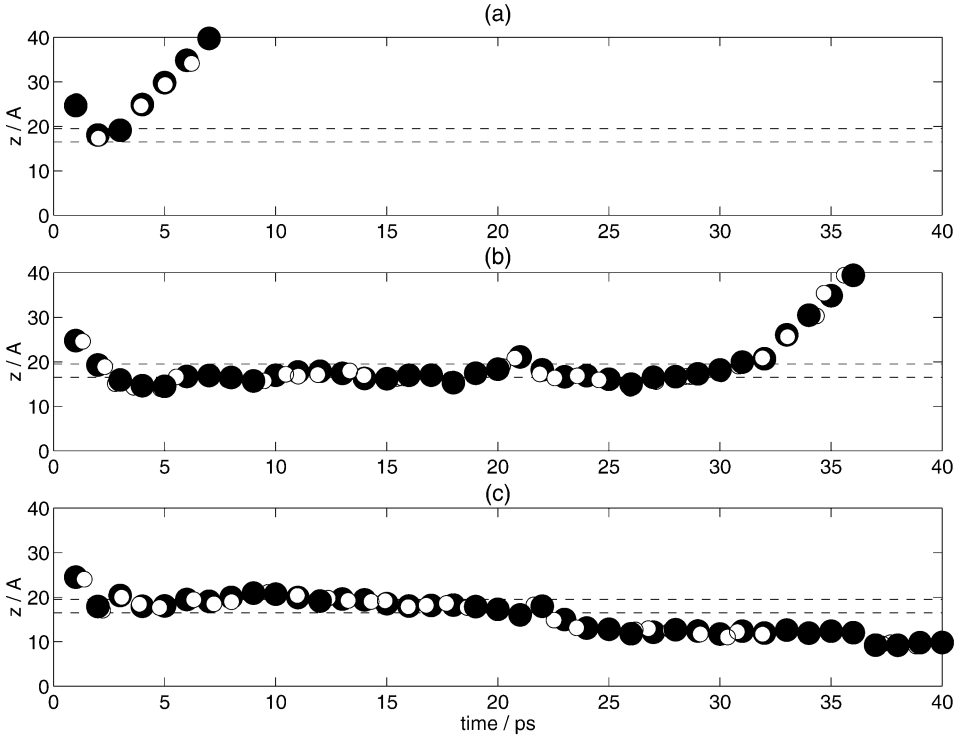

Figure 1. Example of three types of trajectories in scattering simulations: (a) direct scattering, (b) adsorption with subsequent desorption, (c) adsorption with subsequent uptake into the bulk liquid. Dashed lines indicate the interfacial region; solid circles represent oxygen, and open circles represent hydrogen.

3. Results and Discussion

The scattering simulations, described in detail in the previous section, start with a OH radical or an O_3 molecule in the gas phase approaching the liquid/air interface with a thermal velocity. Upon hitting the surface, the particle can either scatter back into the gas phase or become adsorbed at the surface. Once adsorbed, the molecule can remain in the interface, desorb, or become solvated in the liquid bulk (absorbed). A fully solvated molecule can remain in the bulk or return back to the interface across which it originally crossed into the bulk. Because of the slab geometry of the system with two interfaces, it can also diffuse toward the other interface and, eventually, desorb into the gas phase on the other side of the slab. As an illustration, three trajectories for the OH radical interacting with the slab of a saturated NaCl solution are shown in Figure 1. The first trajectory corresponds to direct scattering. The remaining two panels represent "sticking" trajectories, either with a later desorption back into the gas phase or an uptake into the bulk.

3.1. Trapping. Out of 125 trajectories for the OH (O_3) interacting with each of the three slabs, we found direct scattering for 18 (17) trajectories in the case of the saturated NaCl solution/air interface, 8 (17) trajectories in the case of the neat water/air interface, and 11 (5) trajectories in the case of 1.2 M NaI solution/air interface. For all systems under study, the scattering/adsorption probability is almost independent of the incident angle, with direct scattering being slightly more probable for larger impact angles (grazing collisions). Figure 2 shows three sets of trajectories for the OH radical approaching different surfaces at an impact angle of 0° (i.e., perpendicular to the surface). The upper panel corresponds to the saturated NaCl solution/air interface, the middle panel to the neat water/air interface, and the lower panel to the 1.2 M NaI solution/air interface. Analogous sets of trajectories for O_3 are presented in Figure 3. For each trajectory, the *z*-coordinate of the O atom of the OH species (the central O atom in the case of O_3), is plotted against time. For both OH and O_3, direct scattering occurs only for a small fraction of trajectories. For most of the trajectories, these species are at least temporarily adsorbed at the surface and, in some cases (almost exclusively for OH), become later fully solvated. The residence times of the solute, before desorbing back into the gas phase, span a large interval, from a few picoseconds to >100 ps, which is a technical limit given by the length of the simulations. Distributions of the residence times of the OH radical for the three slabs are presented in Figure 4, whereas analogous distributions for O_3 are shown in Figure 5.

A comparison between Figures 2 and 3, as well as Figures 4 and 5, clearly reveals a difference between the behavior of the OH radical and the O_3 molecule. The basic message is that, on average, O_3 desorbs from the surface much faster than OH. Most of the ozone molecules leave the slab within 20−30 ps from the first contact with the surface, whereas a large fraction of the OH radicals remains adsorbed for the entire duration of the simulations. This difference between the OH radical and the O_3 molecule can be quantified by evaluating the mean residence time ($\bar{\tau}$) of the two species on the various surfaces. Table 2 shows that, for all three slabs, the mean residence times of O_3 are less than half of those of OH.

The integral residence probability $P(t)$, i.e., the probability of the gas particle being trapped on the surface or in bulk of the slab for *at least* time *t* before desorbing back to the gas phase, was evaluated for all systems under study. The assessment of trapping was based on the SASA analysis (see Section 2). The solute molecule was considered to be trapped as long as its solvent-accessible surface area corresponded to partial or full solvation. If the solute became fully exposed in the gas phase for a period of >2 ps, it was considered desorbed. The results, for both OH and O_3, comparing the salt solutions to neat water, are presented in Figure 6. For all three slabs, the ozone signals decay much faster than those of the OH radical,

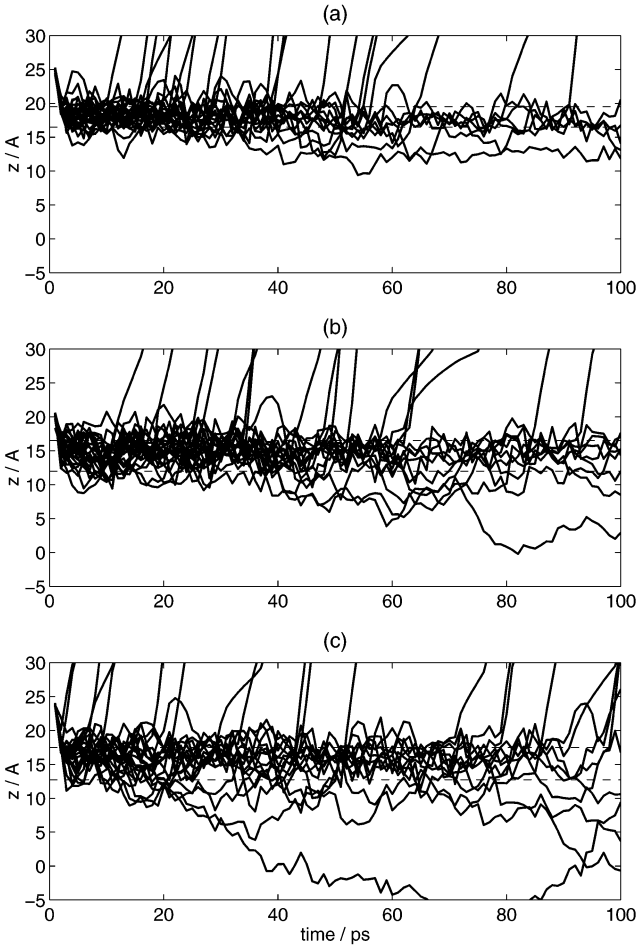

Figure 2. Three sets of trajectories (25 trajectories each) for the OH radical approaching different surfaces at an impact angle of 0° (i.e., perpendicular to the surface). Scattering from (a) the saturated NaCl solution, (b) neat water, and (c) the 1.2 M NaI solution. For each trajectory, the *z*-coordinate of the O atom of the OH radical is plotted against time. Dashed lines define the interfacial layer.

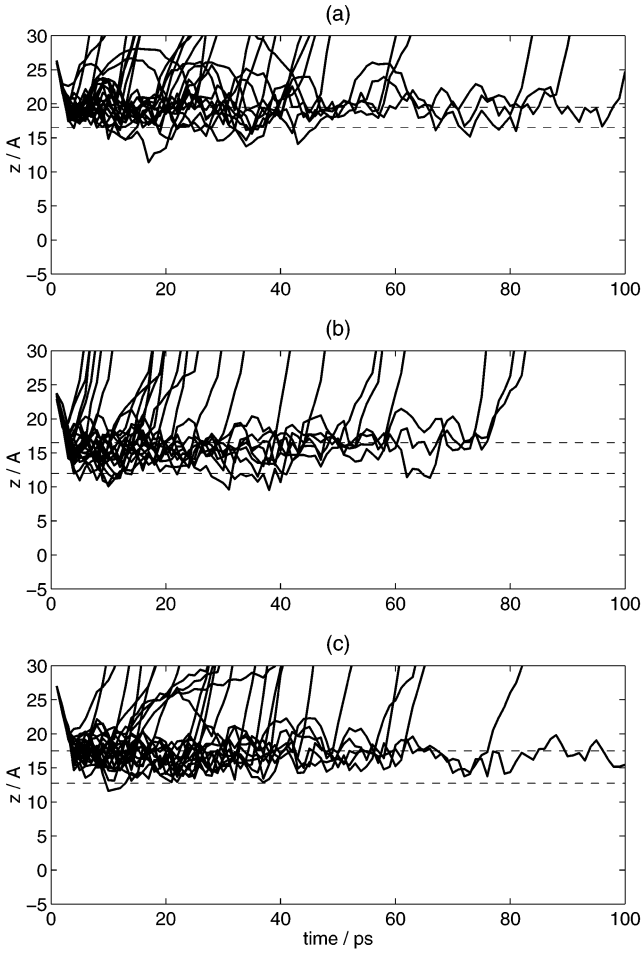

Figure 3. Three sets of trajectories (25 trajectories each) for O_3 approaching different surfaces at an impact angle of 0° (i.e., perpendicular to the surface). Scattering from (a) the saturated NaCl solution, (b) neat water, and (c) the 1.2 M NaI solution. For each trajectory, the *z*-coordinate of the central O atom of O_3 is plotted against time. Dashed lines define the interfacial layer.

which corresponds to a more-rapid ozone desorption from the surfaces. Somewhat surprisingly, the effect of the dissolved salt is rather small, especially in the case of ozone. For OH, the presence of I ions in the interface leads to a slight enhancement of trapping in the region of longer residence times ($t > 50$ ps). However, desorption of OH from the saturated NaCl slab surface back into the gas phase is somewhat faster than from the neat water surface.

The probability that a gas-phase molecule is accommodated on a liquid droplet is commonly expressed using the mass accommodation coefficient (α). On the basis of scattering simulations, α can be defined as follows:

$$\alpha = \frac{\text{number of sticking trajectories}}{\text{total number of trajectories}} \qquad (1)$$

Note that also somewhat different definitions of the mass accommodation coefficient exist in the literature,[37,38] leading possibly to different values of α.

To use this definition, one must specify the minimal residence time τ_{res} of the adsorbate at the surface for a "sticking" trajectory. Mass accommodation coefficients for all systems under study are presented in Table 3 for four different minimal residence times (3, 10, 50, and 90 ps). We see that, because of the desorption that occurs during the course of the simulations (see Figures 2, 3, and 6), increasing τ_{res} significantly reduces the evaluated α values. Obviously, if the desorption back to the gas phase is not negligible, expression (1) does not provide a unique definition of α in the realm of scattering MD simulations. As discussed in detail in ref 36, unlike the experimentally determined values that have a tendency to represent a lower bound of the α value, the present scattering MD simulations provide an upper bound. In addition, the much stronger tendency of O_3—compared to OH—to desorb from the surface reflects itself in the calculated α values only for longer τ_{res} values. Also, evaluated numbers of sticking trajectories that use a longer minimal residence time ($\tau_{res} = 90$ ps for the OH radical and $\tau_{res} = 50$ ps for the O_3 molecule) lead to mass accommodation coefficients that approach (from above) the experimental values $\alpha(OH) = 0.1$[39] and $\alpha(O_3) = 0.04$[40] or $\alpha(O_3) > 0.02$.[41]

3.2. Absorption. Another profound difference between the behavior of the OH radical and O_3 concerns their propensity for bulk solvation. The probability that an O_3 molecule, after having been adsorbed at the interface, becomes fully solvated in the bulk is very small for all slab systems. A trajectory has been classified as "absorption" if the solute has been fully solvated for >5 ps. Only one such trajectory, with a 15-ps bulk solvation of O_3, was observed for the saturated NaCl solution slab, and two such trajectories (45 and 68 ps) were observed for the 1.2 M NaI slab. No trajectory of this type has been found for O_3 on a neat water slab.

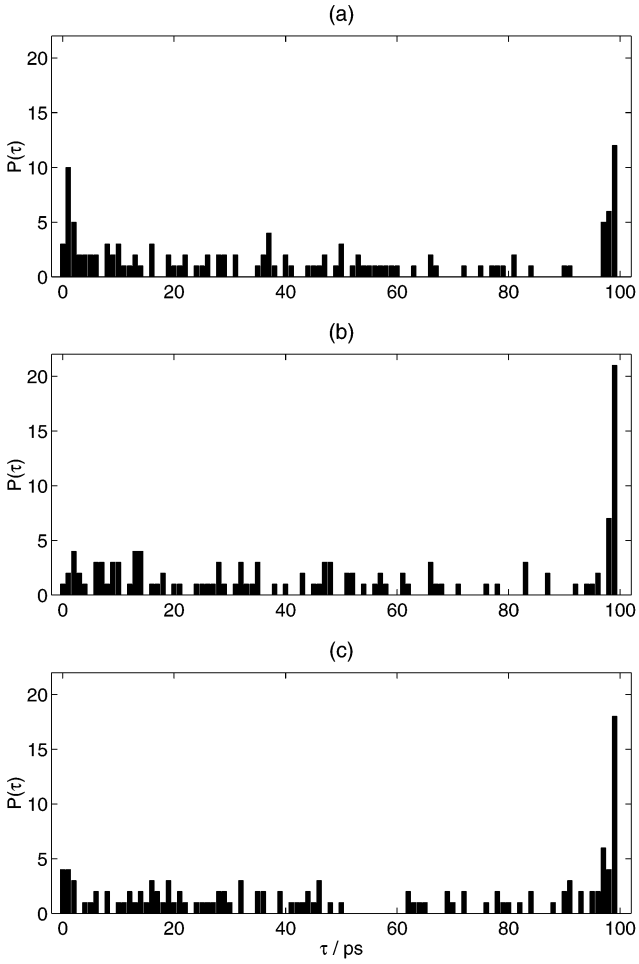

Figure 4. Distribution of residence times of the OH radical at or in (a) the saturated NaCl solution, (b) neat water, and (c) the 1.2 M NaI solution.

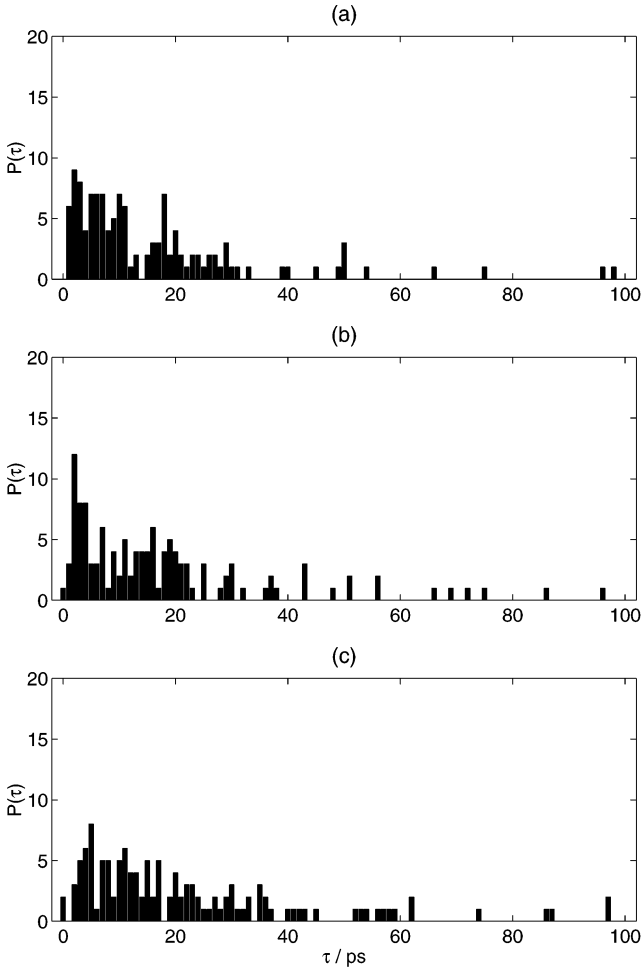

Figure 5. Distribution of residence times of O_3 at or in (a) the saturated NaCl solution, (b) neat water, and (c) the 1.2 M NaI solution.

TABLE 2: Mean Residence Times

	$\bar{\tau}$ (ps)
OH @ NaCl slab	43.0
OH @ water slab	50.4
OH @ NaI slab	53.0
O_3 @ NaCl slab	16.2
O_3 @ water slab	18.1
O_3 @ NaI slab	22.0

However, bulk solvation of the OH radical has been observed for a substantially larger fraction of trajectories: 8 in the case of the saturated NaCl solution, 20 for neat water, and 33 for the 1.2 M NaI slab. The mean solvation times of the OH radical in the two salt solutions are rather similar (28 ps in the saturated NaCl solution, 25.4 ps in the 1.2 M NaI solution) and somewhat longer than that in neat water (17.5 ps). Of the three slabs, the OH species is solvated most easily in aqueous NaI; i.e., the presence of I ions in the solution enhances the uptake of the OH radical into the bulk. This is different from the case of the NaCl solution, where a OH radical remains more confined to the interface region than it does in neat water. As a consequence, OH desorption back into the gas phase is faster from a NaCl solution than from neat water. However, one should remember that this effect might be partly due to inaccuracies in the present force field (slightly overestimated H_2O-Cl^- and underestimated $OH-Cl^-$ interactions, as discussed in Section 2).

3.3. Density Profiles. A useful way of visualizing the occurrence of the solutes at the surface or in the bulk, as well as obtaining the typical depth of penetration of the solutes into the slabs, is to calculate density profiles along the direction perpendicular to the surface of the slab (*z*-axis). For slab simulations, it is usual to average the density profiles over the two approximately equivalent halves of the slab. In Figures 7 and 8, we show the density profiles of the OH radical and O_3, together with those for the water O atoms, for the three investigated slabs. The interval on the *z*-axis in which the water O-atom signal decreases from the plateau corresponding to the bulk water density to zero correlates with the interfacial region. However, because of the large corrugation of the surface, as well as the presence of the ions in the interface of the salt solution systems, this quantity provides only a qualitative definition of the interface. Depending on the salt concentration, the position of the interfacial layer and its thickness differ slightly for each slab. Nevertheless, we see that surface adsorption dominates in all systems. The signal from the solutes adsorbed at the surface of the salty slabs (especially in the case of the saturated NaCl solution) is shifted slightly more outward, compared to that for neat water. This can be rationalized in terms of the contact with the halide ions in the interfacial layer (see below).

Comparing Figures 7 and 8, we see that the signal of O_3 in the gas-phase region is approximately twice that of the OH radical. This is, in fact, in agreement with the lower α value of O_3, compared to OH. The signal from O_3 in the aqueous bulk is almost zero for all slabs, which indicates very little absorption. Still, an enhancement of O_3 uptake into the bulk of the 1.2 M NaI solution by a factor of $\sim$2, compared to that in neat water,

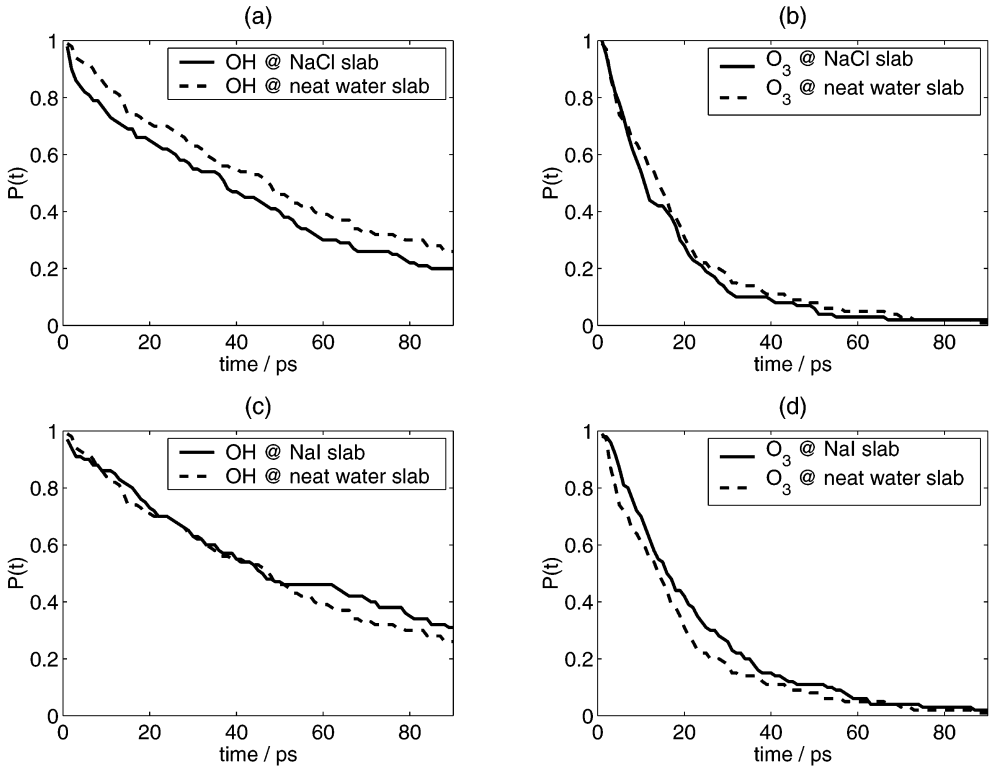

Figure 6. Comparison of integral residence probabilities of the OH radical and O_3 for the salt solution slabs (solid lines) and the neat water slab (dashed lines): (a) OH and the saturated NaCl solution, (b) O_3 and the saturated NaCl solution, (c) OH and the 1.2 M NaI solution, and (d) O_3 and the 1.2 M NaI solution.

TABLE 3: Mass Accommodation Coefficients Calculated for Several Minimal Residence Times, τ_{Res}

	Mass Accommodation Coefficient, α			
	$\tau_{res} = 3$ ps	$\tau_{res} = 10$ ps	$\tau_{res} = 50$ ps	$\tau_{res} = 90$ ps
OH @ NaCl slab	0.86	0.75	0.42	0.20
OH @ water slab	0.94	0.84	0.46	0.26
OH @ NaI slab	0.91	0.86	0.47	0.31
O_3 @ NaCl slab	0.88	0.54	0.06	0.016
O_3 @ water slab	0.87	0.74	0.08	0.008
O_3 @ NaI slab	0.96	0.70	0.11	0.016

can be observed from the bottom panel of Figure 8. The OH radical also prefers interfacial adsorption over bulk solvation. However, this dipolar species solvates in water and aqueous solutions substantially better than the almost-nonpolar O_3 molecule. The OH signal in the interior of the slabs is at least 1 order of magnitude (in the case of the saturated NaCl solution, even 3 orders of magnitude) larger than that of O_3. Finally, a comparison of the three panels of Figure 7 shows that the propensity of the OH radical for the interface is larger in the saturated NaCl solution than in neat water, whereas the opposite is true for that in the 1.2 M NaI solution.

To quantify the aforementioned findings, we used the output of the SASA analysis and calculated the total number of interfacial and bulk configurations (for exact definitions, see Section 1). The resulting numbers, summarized in Table 4, represent the total time, in picoseconds, that the solute spent at the interface or in the bulk, before being desorbed back into the gas phase. The numbers presented in Table 4 are based on the analysis of each individual configuration saved during all simulations, without being possibly biased by assumptions concerning previous definitions of "scattering", "trapping", or "absorption". In this sense, Table 4 contains information that is independent of the trajectory-based quantities previously discussed. Nevertheless, this complementary approach leads to conclusions that are fully consistent with the results previously presented.

The total time the solute was trapped by a given slab (either at the interface or in the bulk) is approximately twice as long for the OH radical than for O_3. This correlates very well with the calculated mean trapping times (see Table 2). The difference between the two solutes, in terms of the total time spent inside the bulk, is even larger (at least 1 order of magnitude). This is in accord with the poor aqueous solubility of O_3, compared to the OH radical (Henry's law constant of O_3 is on the order of 10^{-2} M/atm, whereas the values for the OH radical reported in the literature are in the range of $2.5 \times 10^1 - 9.0 \times 10^3$ M/atm).[42] A difference in sticking to the surface of water, as well as in the aqueous solvation between the two species, can also be expected, on the basis of a comparison of their interaction energy with a single water molecule that is substantially lower for O_3 than for the OH radical. Ab initio calculations of the binding energy of $OH\cdots H_2O$ and $O_3\cdots H_2O$ complexes yielded values of $\Delta E_{OH\cdots H_2O} = 4.9$ kcal/mol and $\Delta E_{O_3\cdots H_2O} = 1.6$ kcal/mol.[45] A similar difference exists between the hydration energies of the two species, which were reported to be 8.5 kcal/mol for the OH radical[43] and 5.8 kcal/mol for O_3.[44]

A somewhat faster desorption of the OH radical from the saturated NaCl solution surface, compared to that from the other two slabs, manifests itself in the smaller number of "trapped" configurations in this case. The trapping of O_3 at the surface is almost the same for all three slabs; however, the uptake of O_3 into the bulk is enhanced by more than 1 order of magnitude by the presence of I ions in the solution, compared to that for neat water, in agreement with the results of recent experimental studies.[41,45] The enhancement of bulk solvation in the NaI solution is pronounced also in the case of OH.

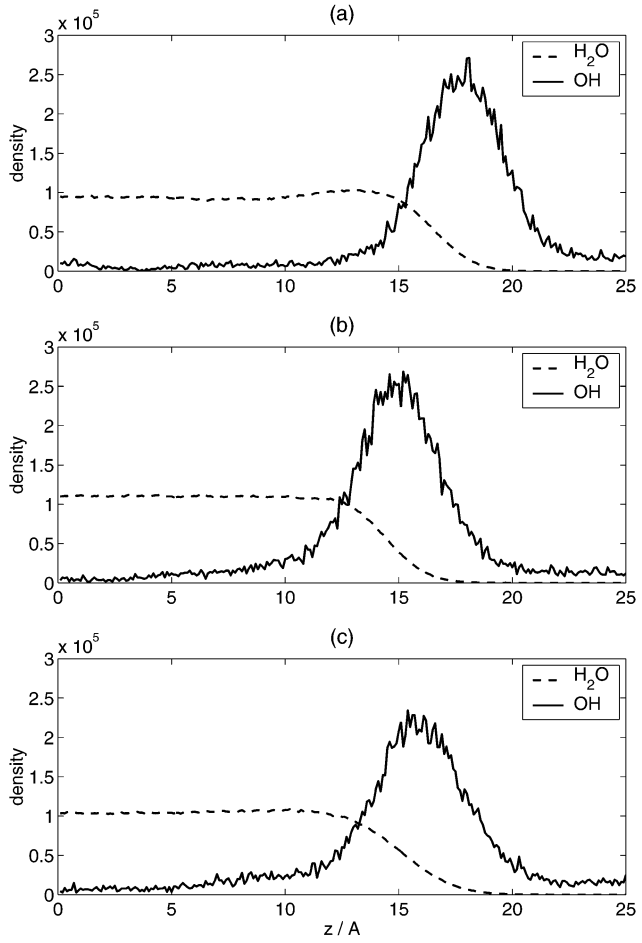

Figure 7. Density profiles of the OH radical at (a) the saturated NaCl solution, (b) neat water, and (c) the 1.2 M NaI solution. Dashed lines denote the density profiles of water O atoms.

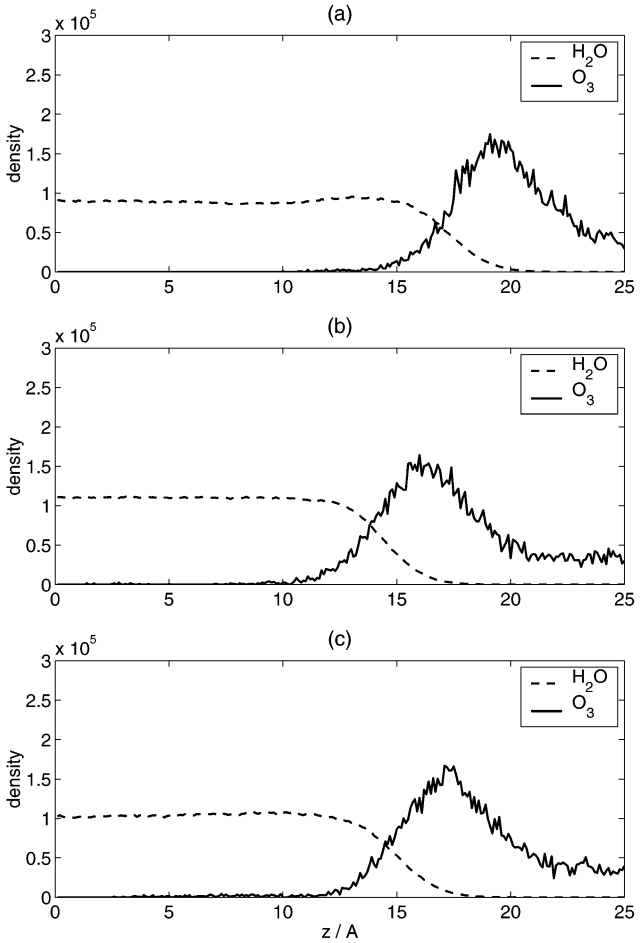

Figure 8. Density profiles of O_3 at (a) the saturated NaCl solution, (b) neat water, and (c) the 1.2 M NaI solution. Dashed lines denote the density profiles of water O atoms.

3.4. Orientational Effects. In the interfacial region, there is a strong preference for the OH radical to be parallel to the surface or to be oriented perpendicular to the surface with the H atom pointing toward the slab. This orientational effect of the interface on the OH radical is clearly visible in all three trajectories depicted in Figure 1. In an attempt to demonstrate this effect in a more quantitative way, we plotted in Figure 9, the orientational distribution $P(\cos\theta)$ of the O → H bond vector, with respect to the surface normal (see Figure 9). The upper panel of Figure 9 corresponds to the saturated NaCl solution slab, the middle panel corresponds to the neat water slab, and the lower panel corresponds to the 1.2 M NaI solution slab. The orientational probability distributions for the gas phase, the interface, and the bulk were obtained by averaging separately over each of the corresponding set of configurations, as defined in Section 2.

As expected, the orientation of the OH radical in the gas phase, as well as in the bulk, is entirely random and is, therefore, described by a uniform probability distribution. However, all the probability distributions describing the interfacial configurations exhibit a pronounced minimum for $\cos\theta = 1$ (where θ is the angle between the O → H bond vector and the surface normal). Thus, in the interface, the O atom of the OH radical tends to point away from the slab. In the neat water case, the probability distribution for the interface peaks at $\cos\theta \approx -1$, which corresponds to the O−H bond being perpendicular to the surface, with the H atom facing toward the bulk. The analogous distributions for the two salt solutions exhibit a plateau region between $\cos\theta = -1$ and $\cos\theta = 0$, suggesting that there is an almost equal probability for any orientation of the OH radical between the O−H bond being perpendicular to the surface (with the H atom facing the slab) and the O−H bond being parallel with the surface. The observed behavior of the OH radical is clearly connected with the orientation of water molecules themselves in the interfacial layer.[27,46]

TABLE 4: Total Time Spent in Interface/Bulk

	Time Spent (ps)	
	at interface	in bulk
OH @ NaCl slab	5199	317
OH @ water slab	6044	783
OH @ NaI slab	5509	1400
O_3 @ NaCl slab	2784	12
O_3 @ water slab	2887	4
O_3 @ NaI slab	2857	115

3.5. Surface Solvation and Contact of OH with Halide Ions. We used the simulations to gain microscopic insight into the (partial) solvation of the two species under study in the interfacial region. First, we evaluated, for each case, the solute−halide, solute−sodium, and solute−water oxygen radial distribution functions (RDFs), taking into account all configurations when the solute was situated in the interface. The RDFs were calculated from the geometrical center of the solute, i.e., from the center of the O−H bond or, in the case of O_3, from the center of the $O_1-O_2-O_3$ triangle. In Figure 10, the resulting curves for the OH radical adsorbed at the surface of both saturated NaCl solution and 1.2 M NaI solution are presented. For both solutions, the peaks corresponding to the halide ions

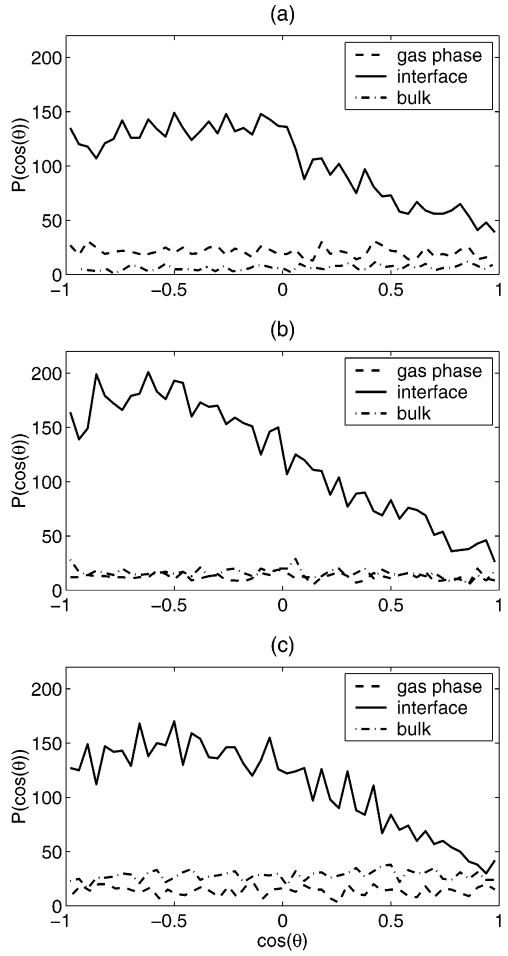

Figure 9. Orientational distributions of the O → H vector, relative to the surface normal for (a) the saturated NaCl solution, (b) neat water, and (c) the 1.2 M NaI solution. Dashed lines represent the orientation of the OH radical in the gas phase above the surface, solid lines represent the orientation of the OH radical in the interfacial layer, and dash−dotted lines represent the orientation of the OH radical in the bulk liquid; cos $\theta = 1$ corresponds to the O → H vector parallel to the surface normal with the H atom pointing away from the interface, cos $\theta = 0$ corresponds to the O → H vector being perpendicular to the surface normal, and cos $\theta = -1$ corresponds to the H atom facing the surface.

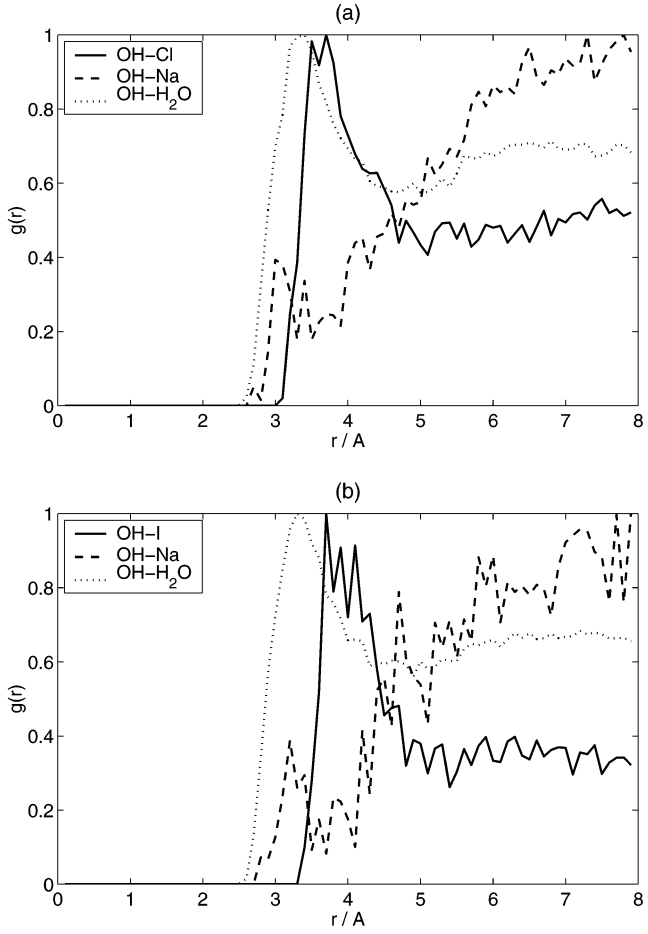

Figure 10. Radial distribution functions (RDFs) for the OH radical adsorbed at the interface of (a) the saturated NaCl solution and (b) the 1.2 M NaI solution. Solid line corresponds to the OH−X^- RDF (X = Cl, I), dashed line corresponds to the OH−Na^+ RDF, and dotted line corresponds to the OH−water O atom RDF. RDFs have been evaluated from the center of the O−H bond.

and water O atoms in the first solvation shell around the OH radical are pronounced. The Na^+ ions are almost absent from the interfacial layer, which results in the suppression of the first peak on the OH−Na RDFs. Analogical RDF curves for ozone are shown in Figure 11. Because of the fact that O_3 molecules spend much less time at the interface than OH radicals, the curves in Figure 11 have poorer statistics, compared to those in Figure 10. Nevertheless, the peaks corresponding to the nearest water molecules, and in the case of the saturated NaCl slab, also to the nearest Cl^- ions, are well-resolved. In the case of the 1.2 M NaI slab, the poor I statistics leads to a noisy RDF signal, from which the first peak at ∼5 Å but not the first subsequent minimum can be identified.

To address the question of the contact between the OH radical and the halide ions that are present in the surface layer of the salt solution, we analyzed all configurations recorded in the course of the simulations, for which the OH radical was located in the interface. For each configuration, we calculated the number of water molecules and halide ions in the first solvation shell of the OH radical, i.e., the number of particles for which their distance from the center of the O−H bond fell below a certain threshold. The critical values were set to 5.1 Å for OH−Cl^-, 5.5 Å for OH−I^-, and to 5.0 Å for OH−water O atom, which correspond to minima after the first peaks of the corresponding RDFs (see Figure 10). By averaging over all surface configurations, we evaluated the average number of nearest neighbors of the OH radical located in the interfacial layer. The results (see Table 5) indicate that a OH radical, trapped at the surface of the salt solution, is, on average, surrounded by slightly less than six water molecules. In addition to water molecules, the OH radical is in direct contact with a Cl^- ion (in the saturated NaCl slab) ∼60% of the time or is in contact with an I^- ion (in the 1.2 M NaI slab) ∼30% of the time. Simultaneous contact with more than one halide ion occurred in a negligible number of configurations. We have also recorded the length of each contact between the OH radical and a halide ion. A distribution of the contact times t_{cont} is presented in Figure 12. In most of the cases, the OH−X^- contact lasted 1−5 ps. The average contact time was 2.9 ps for OH−Cl^- and 2.25 ps for OH−I^-. However, in some cases, the OH−X^- contact was substantially prolonged. Approximately 20% of the OH−Cl^- contact events had a duration of >5 ps, and 3% had a duration of >10 ps. The maximum duration of the contact reached almost 20 ps. In regard to the OH−I^- contacts, 10% had a duration of >5 ps and 1% had a duration of >10 ps, with a maximum duration somewhat below 15 ps.

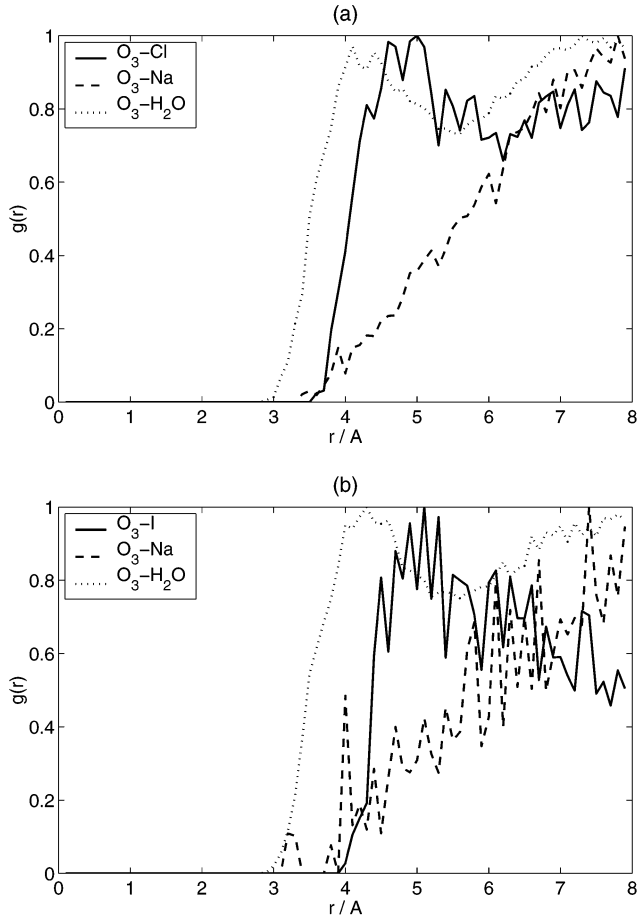

Figure 11. RDFs for O_3 adsorbed at the interface of (a) the saturated NaCl solution, and (b) the 1.2 M NaI solution. Solid line corresponds to the O_3-X^- RDF (X = Cl, I), dashed line corresponds to the O_3-Na^+ RDF, and dotted line corresponds to the O_3-water O atom RDF. RDFs have been evaluated from the center of the $O_1-O_2-O_3$ triangle.

TABLE 5: Average Number of Halide Ions (X = Cl, I) and Water Molecules in the First Solvation Shell of OH in Interface

	Average Number of Ions or Molecules	
	X^-	H_2O
OH @ NaCl slab	0.61	5.70
OH @ NaI slab	0.28	6.41

Contacts between OH and Cl^- are also seen in a series of snapshots from a typical "sticking" trajectory of OH at the saturated NaCl solution surface (the same trajectory as in Figure 1b), shown in Figure 13. In this particular trajectory, the OH radical initially "landed" on a part of the surface that was covered by water molecules. Within 6 ps, it migrated to a Cl^- ion and stayed in the vicinity of which for the next 10 ps. At $t \approx 20$ ps, the OH radical then raised slightly above the interface and jumped to another part of the surface. There, subsequent contacts with three different Cl^- ions occurred (for 3, 1, and 4 ps, respectively) before OH desorption back into the gas phase. The last panel in Figure 13 shows the entire trajectory of the OH radical at the surface (in the *xy*-plane). This figure demonstrates the mobility of the OH radical trapped at the surface of the aqueous salt solution, as well as the rather-high probability of its contact with Cl^- ions present in the interface. We see an essentially diffusive motion of the OH radical in the interface, with Cl^- anions serving as weak attractors.

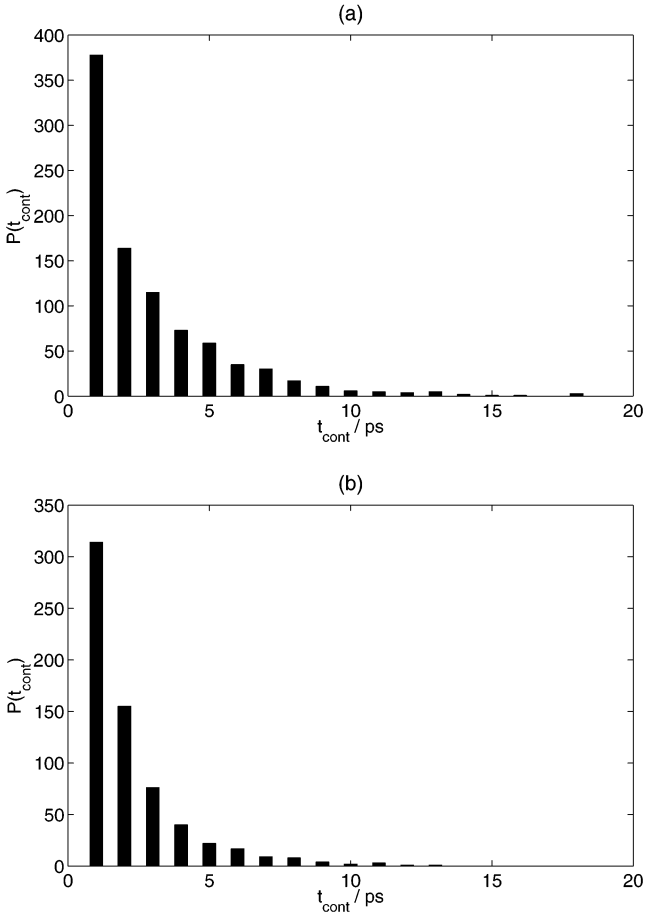

Figure 12. Distribution of contact times of OH with (a) Cl^- ions in the interface of the saturated NaCl solution and (b) I^- ions in the interface of the 1.2 M NaI solution.

4. Conclusions

We have investigated, using molecular dynamics simulations, collisions of the hydroxyl (OH) radical and ozone (O_3) with the surface of neat water and that of a sodium chloride (NaCl) or sodium iodide (NaI) solution. For both gaseous species, we have found substantial trapping. On average, the OH radical stays at the interface much longer and has also a higher probability to solvate into the bulk than O_3. Also, at the interface, the OH radical becomes oriented with hydrogen, rarely pointing away from the aqueous bulk. Somewhat surprisingly to us, the effect of the dissolved salt on the trapping of the OH radical or O_3 is very small. It follows from our simulations that there are, however, frequent and sufficiently long contacts between OH and Cl^- species in the interfacial layer to make the production of molecular chlorine (Cl_2) from the aqueous sea-salt particles via the $OH\cdots Cl^-$ complex plausible.[19] The present work thus provides strong evidence in favor of the suggested *surface* mechanism of this reaction. This is further supported by recent experiments,[47] in which an increase of OH^- concentration in the aqueous sea-salt aerosol particles has been observed as a result of Cl_2 production by the photolysis of O_3 in the presence of salt particles above their deliquescence point.

One of the main conclusions of our study is that both OH and O_3 prefer surface adsorption over bulk solvation in water, as well as in salt solutions. This finding sheds new light onto a broad variety of processes in the troposphere. The high probability of surface reactions has important implications for chemistry in the marine boundary layer, as well as above the arctic snow packs at polar sunrise.[48] Therefore, the incorporation

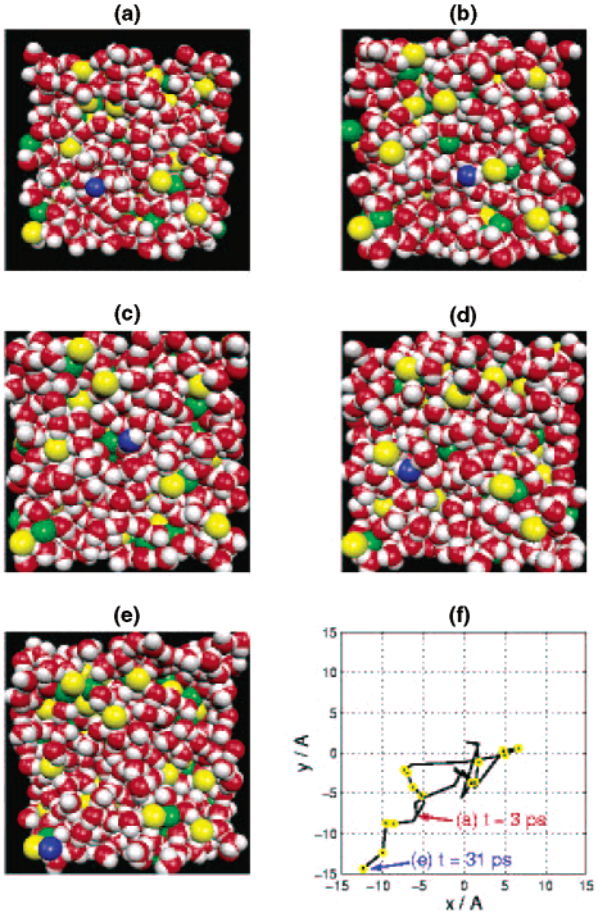

Figure 13. Panels a−e show a series of snapshots from a typical "sticking" trajectory, showing the OH radical adsorbed at the surface of the saturated NaCl solution. Color coding: gray = hydrogen, blue = OH oxygen, red = water oxygen, yellow = Cl^-, green = Na^+. Panel f shows the entire trajectory projected into the *xy*-plane. Yellow circles indicate contacts of OH with Cl^-.

of heterogeneous chemistry into atmospheric models is imperative for improving their performance.

Acknowledgment. The authors thank Barbara Finlayson-Pitts and Donald Dabdub for helpful discussions pertaining to this study. Support from the National Science Foundation (NSF), via Grant No. CHE-0209719, is gratefully acknowledged. Work at the Hebrew University was supported by the Israel Science Foundation (ISF) via Grant No. 127/00-3 to R.B.G. The Center for Complex Molecular Systems and Biomolecules is supported by the Czech Ministry of Education (through Grant No. LN00A032).

Note Added after ASAP Posting. This article was posted ASAP on 10/28/2003. A change has been made in the column heading of the fourth column in Table 1. The correct version was posted on 11/6/2003.

References and Notes

(1) Wayne, R. P. In *Chemistry of Atmospheres*; Oxford University: Oxford, U.K., 2000.
(2) Finlayson-Pitts, B. J.; Pitts, J. N. In *Chemistry of the Upper and Lower Atmosphere*; Academic Press: San Diego, CA, 2000.
(3) Oum, K. W.; Lakin, M. J.; DeHaan, D. O.; Brauers, T.; Finlayson-Pitts, B. J. *Science* **1998**, *279*, 74.
(4) Vogt, R.; Crutzen, P. J.; Sander, R. *Nature* **1996**, *383*, 327.
(5) Finlayson-Pitts, B. J.; Ezell, M. J.; Pitts, J. N., Jr. *Nature (London)* **1989**, *337*, 241.
(6) Andreae, M. O.; Crutzen, P. J. *Science* **1997**, *221*, 744.
(7) Levy, D. J.; Lee, A. M.; Toumi, R.; Newchurch, M. J.; Pirre, M.; Renard, J. B. *J. Geophys. Res.* **1997**, *102*, 3671.
(8) Chameidas, W. L.; Davis, D. D. *J. Geophys. Res.* **1982**, *87*, 4863.
(9) Hendrick, J.; Lippert, E.; Petry, H.; Ebel, A. J. *J. Geophys. Res.* **1999**, *104*, 5531.
(10) Ellison, G. B.; Tuck, A. F.; Vaida, V. *J. Geophys. Res.* **1999**, *104*, 11633.
(11) Barker, J. A.; Auerbach, D. J. *Surf. Sci. Rep.* **1984**, *4*, 1.
(12) Gerber, R. B. *Chem. Rev.* **1987**, *87*, 29.
(13) Rettner, C. T.; Auerbach, D. J.; Tully, J. C.; Kleyn, A. W. *J. Phys. Chem.* **1996**, *100*, 31.
(14) Nathanson, G. M.; Davidovits, P.; Wornsop, D. R.; Kolb, C. E. *J. Phys. Chem.* **1996**, *100*, 31.
(15) Saecker, M. E.; Govoni, S. T.; Kowalski, D.; King, H. E.; Nathanson, G. M. *Science* **1991**, *252*, 1421.
(16) Saecker, M. E.; Nathanson, G. M. *J. Chem. Phys.* **1994**, *100*, 3999.
(17) Lipkin, N.; Gerber, R. B.; Moiseyev, N.; Nathanson, G. *J. Chem. Phys.* **1994**, *100*, 8408.
(18) Benjamin, I.; Wilson, M. A.; Pohorille, A.; Nathanson, G. M. *Chem. Phys. Lett.* **1995**, *243*, 222.
(19) Knipping, E. M.; Lakin, M. J.; Foster, K. L.; Jungwirth, P.; Tobias, D. J.; Gerber, R. B.; Dabbub, D.; Finlayson-Pitts, B. J. *Science* **2000**, *288*, 301.
(20) Case, D. A.; Pearlman, D. A.; Caldwell, J. W.; Cheatham, T. E., III; Ross, W. S.; Simmerling, C. L.; Darden, T. A.; Merz, K. M.; Stanton, R. V.; Cheng, A. L.; Vincent, J. J.; Crowley, M.; Tsui, V.; Radmer, R. J.; Duan, Y.; Pitera, J.; Massova, I.; Seibel, G. L.; Singh, U. C.; Weiner, P. K.; Kollman, P. A. *AMBER6*; University of California: San Francisco, CA, 1999.
(21) Caldwell, J.; Dang, L. X.; Kollman, P. A. *J. Am. Chem. Soc.* **1990**, *112*, 9144.
(22) Perera, L.; Berkowitz, M. J. *J. Chem. Phys.* **1991**, *95*, 1954.
(23) Perera, L.; Berkowitz, M. J. *J. Chem. Phys.* **1994**, *100*, 3085.
(24) Markovich, G.; Perera, L.; Berkowitz, M. J.; Cheshnovsky, O. *J. Chem. Phys.* **1996**, *105*, 2675.
(25) Tobias, D. J.; Jungwirth, P.; Parrinello, M. *J. Chem. Phys.* **2001**, *114*, 7036.
(26) Jungwirth, P.; Tobias, D. J. *J. Phys. Chem. B* **2000**, *104*, 7702.
(27) Jungwirth, P.; Tobias, D. J. *J. Phys. Chem. B* **2001**, *105*, 10468.
(28) Jungwirth, P.; Tobias, D. J. *J. Phys. Chem. B* **2002**, *106*, 6361.
(29) Pople, J. A.; Head-Gordon, M.; Raghavachari, K. *J. Chem. Phys.* **1987**, *87*, 5968.
(30) Kendall, R. A.; Dunning, T. H., Jr.; Harrison, R. J. *J. Chem. Phys.* **1992**, *96*, 6796.
(31) Woon, D. E.; Dunning, T. H., Jr. *J. Chem. Phys.* **1993**, *98*, 1358.
(32) Frisch, M. J.; Trucks, G. W.; Schlegel, H. B.; Scuseria, G. E.; Robb, M. A.; Cheeseman, J. R.; Zakrzewski, V. G.; Montgomery, J. A., Jr.; Stratmann, R. E.; Burant, J. C.; Dapprich, S.; Millam, J. M.; Daniels, A. D.; Kudin, K. N.; Strain, M. C.; Farkas, O.; Tomasi, J.; Barone, V.; Cossi, M.; Cammi, R.; Mennucci, B.; Pomelli, C.; Adamo, C.; Clifford, S.; Ochterski, J.; Petersson, G. A.; Ayala, P. Y.; Cui, Q.; Morokuma, K.; Malick, D. K.; Rabuck, A. D.; Raghavachari, K.; Foresman, J. B.; Cioslowski, J.; Ortiz, J. V.; Stefanov, B. B.; Liu, G.; Liashenko, A.; Piskorz, P.; Komaromi, I.; Gomperts, R.; Martin, R. L.; Fox, D. J.; Keith, T.; Al-Laham, M. A.; Peng, C. Y.; Nanayakkara, A.; Gonzalez, C.; Challacombe, M.; Gill, P. M. W.; Johnson, B. G.; Chen, W.; Wong, M. W.; Andres, J. L.; Head-Gordon, M.; Replogle, E. S.; Pople, J. A. *Gaussian 98*, revision A.7; Gaussian, Inc.: Pittsburgh, PA, 1998.
(33) Lee, B.; Richards, F. M. *J. Mol. Biol.* **1971**, *55*, 379.
(34) Ryckaert, J.-P.; Ciccotti, G.; Berendsen, H. J. C. *J. Comput. Phys.* **1977**, *23*, 327.
(35) Essmann, U.; Perera, L.; Berkowitz, M. L.; Darden, T.; Pedersen, L. G. *J. Chem. Phys* **1995**, *103*, 8577.
(36) Wilson, M. A.; Pohorille, A. *J. Phys. Chem. B* **1997**, *101*, 3130.
(37) Taylor, R. S.; Ray, D.; Garrett, B. C. *J. Phys. Chem. B* **1997**, *101*, 5473.
(38) Taylor, R. S.; Garrett, B. C. *J. Phys. Chem. B* **1999**, *103*, 844.
(39) Frost, G. J.; Trainer, M.; Mauldin, R. L.; Eisele, F. L.; Prevot, A. S. H.; Flocke, S. J.; Madronich, S.; Kok, G.; Schillawski, R. D.; Baumgardner, D.; Bradshaw, J. *J. Geophys. Res., [Atmos.]* **1999**, *104*, 16041.
(40) Muller, B.; Heal, M. R. *Phys. Chem. Chem. Phys.* **2002**, *4*, 3365.
(41) Schutze, M.; Herrmann, H. *Phys. Chem. Chem. Phys.* **2002**, *4*, 60.
(42) Sander, R. *Compilation of Henry's Law Constants for Inorganic and Organic Species of Potential Importance in Environmental Chemistry*; www.mpch-mainz.mpg.de/~sander/res/henry.html, and references therein.
(43) Coe, J. V.; Earhart, A. D.; Cohen, M. H.; Hoffman, G. J.; Sarkas, H. W.; Bowen, K. H. *J. Chem. Phys.* **1997**, *107*, 6023.
(44) Lin, J.; Nakajima, T. *THEOCHEM* **2003**, *625*, 161.
(45) Magi, L.; Schweitzer, F.; Pallares, C.; Cherif, S.; Mirabel, P.; George, C. *J. Phys. Chem. A* **1997**, *101*, 4943.
(46) Taylor, R. S.; Dang, L. X.; Garrett, B. C. *J. Phys. Chem.* **1996**, *100*, 11720.
(47) Laskin, A.; Gaspar, D. J.; Wang, W.; Hunt, S. W.; Covin, J. P.; Colson, S. D.; Finlayson-Pitts, B. J. *Science* **2003**, *301*, 340.
(48) Finlayson-Pitts, B. J.; Hemminger, J. C. *J. Phys. Chem. A* **2000**, *104*, 11463.